

Rate processes in nonlinear optical dynamics with many attractors

F. T. Arecchi

Physics Department, University and Istituto Nazionale di Ottica, Florence, Italy

(Received 26 April 1991; accepted for publication 16 July 1991)

Kramers' 1940 paper and its successive elaborations have extensively explored the transition rate between two stable situations, that is, in the language of system dynamics, the transition between the basins of attraction of two stable fixed point attractors. In a nonequilibrium system some of the above conditions may be violated, either because one of the two fixed points is unstable, as in the case of transient phenomena, or because both fixed points are unstable, as in the case of heteroclinic chaos, or because the attractors are more complex than fixed points, as in a chaotic dynamics where two or more strange attractors coexist. Furthermore, there is recent experimental evidence of space-time complexity consisting in the alternate or simultaneous oscillation of many modes, each one with its own (possibly chaotic) dynamics. In all the above cases, coexistence of many alternative paths implies a choice, either due to noise or self-triggered by the same interacting degrees of freedom. A review of the above phenomena in the case of nonequilibrium optical systems is here presented, with the aim of stimulating theoretical investigation on these novel rate processes.

I. INTRODUCTION

The emergence of correlated space-time structures in systems away from thermal equilibrium is a subject of current interest in many areas of natural sciences such as biology, hydrodynamics, chemical reactions, plasma physics, optics, and computer science. This emergence should be called "organization" rather than "self-organization," to stress the fact that any new pattern implies a dynamical bifurcation, thus some variation in a control parameter, which is anyway extrinsic to the organizing system.¹ Furthermore any bifurcation implies a selection between alternative choices.

In its simplest form, this selection problem motivated Kramers' 1940 paper on the rate process between two stable energy minima separated by a barrier.² In Sec. XI of their comprehensive review on "Reaction rate theory," Hänggi, Talkner, and Borkovec³ devote a short remark to rate theory in nonequilibrium systems, and particularly to mean first passage time in the decay of initially unstable states. This matter however deserves a more extensive treatment, and here a first formulation is attempted, limiting the examples to optical ones. Precisely, four situations of transitions in nonequilibrium optical systems are presented which have been explored experimentally and which still await a formal treatment in terms of a generalized Kramers transition rate theory.

The reason why this review is limited to optics, besides the obvious limitation of personal competence, is that some of the problems treated in the forthcoming sections were faced for the first time in optical experiments. Laser transition experiments display some advantage as compared with hydrodynamic ones. In the former case the characteristic time scales are in the few microsecond range against the several seconds of a fluid experiment. This allows one to collect a large number of independent data over a time interval short enough to avoid environmental

changes, thus reducing the requirements on stabilization. Furthermore, photon statistics techniques provide a relative precision between 10^{-3} and 10^{-4} , making possible the use of 12 bit digitizers, which may be crucial for reliable assignment of fractal dimensions and Kolmogorov entropies in chaotic measurements.⁴ Finally, while changing the geometry of a fluid experiment (the so-called aspect ratio) requires building new containers, in optics it is very simple to control the cavity length or the pupil aperture by simple settings of mirrors and diaphragms.

In view of this focus on optics, Sec. II introduces a general discussion on space constraints which act as filters in optical systems, reducing the dimensionality of the dynamical space.

Section III reports on the transient features (photon statistics or passage time statistics) associated with the decay out of an unstable state. In this case, one of two fixed points of the Kramers problem has been replaced by an unstable one.

Section IV refers to chaotic laser dynamics, when two or more strange attractors coexist. The jumps from one to another are either noise-induced jumps, or they are induced by a change in a control parameter which lowers the energy barrier separating the two attractors (crises). In both cases the power spectrum has a low-frequency part (jump spectrum) independent from the high-frequency chaotic spectrum which accounts for the decay of correlations within a single attractor.

Section V is devoted to Shil'nikov chaos in optics and to its description in terms of time maps. By Shil'nikov chaos we denote a global dynamics ruled by two (or more) fixed points all unstable, so that the attractor consists in a continuous wandering from one to the other, which is asymptotic to a heteroclinic orbit, or to a looping around only one point without influence of the other ones, which is asymptotic to a homoclinic orbit. The optical Shil'nikov chaos was explored in lasers with feedback. The character-

ization was done in terms of the iteration map of the successive return times to a given surface of section. This may be considered as an extension of the passage time method of Sec. III to the case of multiple passages.

Section VI is devoted to a description of the recent experimental evidence of "chaotic itinerancy," that is, of jump processes among different space configurations, self-triggered by the same dynamics, without external noise or parameter modulation. So far, the corresponding theoretical understanding is based only on numerical simulations.

Besides the transient case of Sec. III, the other sections cover cases of deterministic chaos in dissipative systems, characterized by two features, namely, (i) the dynamics is low-dimensional, that is, the corresponding attractors can be embedded in a low-dimensional phase space, and (ii) many attractors coexist for the same parameter values.

Feature (i) means that the system can be modeled by a small number of nonlinearly coupled ODEs (ordinary differential equations). Even if the physics refers to a distributed field ruled by PDEs (partial differential equations), that means that the relevant motion can be confined to low-dimensional manifolds. Feature (ii) means that repeated preparations of the physical system do not lead to the same attractor, since in general an ensemble of initial conditions is spread over many basins of attraction. As discussed in Sec. IV, even in the evolution from a fixed initial condition, the trajectory can belong successively to different attractors, either because activation by external noise has allowed a jump across a basin boundary, or because external modulation of a control parameter has induced a "crisis" whereby the attractor hits the basin boundary and can go across it without an activation (this would be the equivalent of barrierless transitions).

A new phenomenon, recently introduced theoretically and just observed is that of "chaotic itinerancy." It consists of the successive visit of different slow manifolds with a chaotic dynamics within each of them, persisting for a time much longer than the transition time from one to another. This stems from the interplay of a rather small number of degrees of freedom, without any added noise.

Here, as well as in the above cases, the question arises whether a suitable extension of Kramers' theory might yield the transition rates from one to another slow manifold and the persistence time within each of them.

Due to the novelty of the phenomena here reviewed and to the lack of a formalized rate treatment, the presentation is rather sketchy and introductory. It is hoped that it will stimulate theoretical investigation.

II. SPACE-TIME COMPLEXITY IN NONLINEAR OPTICS

In chemical reactions and in fluid dynamics it is straightforward to scale up the system size from small to large cells, thus making it possible to explore in many ways the passage from systems coherent (fully correlated) in space to systems made up of many uncorrelated, or weakly correlated, domains.

Questions such as the passage from order to chaos within a single domain and possible synchronizations of time behaviors at different space domains, have been ad-

ressed in past years, with the general idea in mind that space-time organization is what makes a large scale object complex. This investigation line has given rise to the so-called space-time complexity.

Thus far, such an investigation was not possible in laser optics, since this was based on the Schawlow-Townes original idea of a drastic mode selection, cutting off all longitudinal and transverse modes but one.⁵

Let us see explicitly how this truncation procedure works in the usual laser geometry. The field $e(r,t)$ obeys the standard wave equation

$$\square^2 e = -\mu \frac{\partial^2 p}{\partial t^2}, \quad (1)$$

where the wave operator is denoted by $\square^2 = \nabla^2 - (1/c^2)(\partial^2/\partial t^2)$ and $p(r,t)$ is the induced polarization. Laser cavities are mainly extended in a z direction. In fact Schawlow and Townes proposed a Fabry-Perot cavity consisting of two mirrors placed in front of one another along a z axis. The field can then be expanded as

$$e(\mathbf{r},t) = E(x,y,z,t) e^{-i(\omega t - kz)}. \quad (2)$$

If the longitudinal variations are mainly accounted for by the plane wave, then we can take the envelope E as slowly varying in t and z with respect to the variation rates ω and k in the plane wave exponential. Furthermore we call P the projection of p on the plane wave. By neglecting second-order envelope derivatives it is easy to approximate the wave operator on E as

$$\square^2 \rightarrow 2ik \left(\partial_z + \frac{1}{c} \partial_t \right) + \partial_x^2 + \partial_y^2 \quad (3)$$

(where ∂_z , ∂_x^2 , etc. are shortened notations for $\partial/\partial z$, $\partial^2/\partial x^2$, etc.). This further suggests three relevant physical situations.

A. (1+0)-dimensional optics

Assuming that the laser cavity is a cylinder of length L , with two mirrors of radius a at the two ends, the cavity resonance spectrum is made of discrete lines separated by $c/2L$ in frequency, each one corresponding to an integer number of half-wavelengths confined within L [Fig. 1(a)], plus a crown of quasidegenerate transverse modes at the same longitudinal wave number, with their propagation vectors separated from each other by a diffraction angle λ/a [Fig. 1(b)].

Take again a line narrower than the longitudinal frequency separation (so-called free spectral range) and a Fresnel number

$$F \equiv a^2/\lambda L$$

of the order of unity, so that the first off-axis mode already escapes out of the mirror. Intuitively F is the ratio between the geometric angle a/L of view of one mirror from the other and the diffractive angle λ/a .

In such a case we can neglect all space derivatives in (3) and reduce the wave operator to a total time derivative $\square^2 \rightarrow 2i\omega \partial_t$. The dynamic system (one time dimension) has no space extension, thus we say that it is (1+0)dimen-

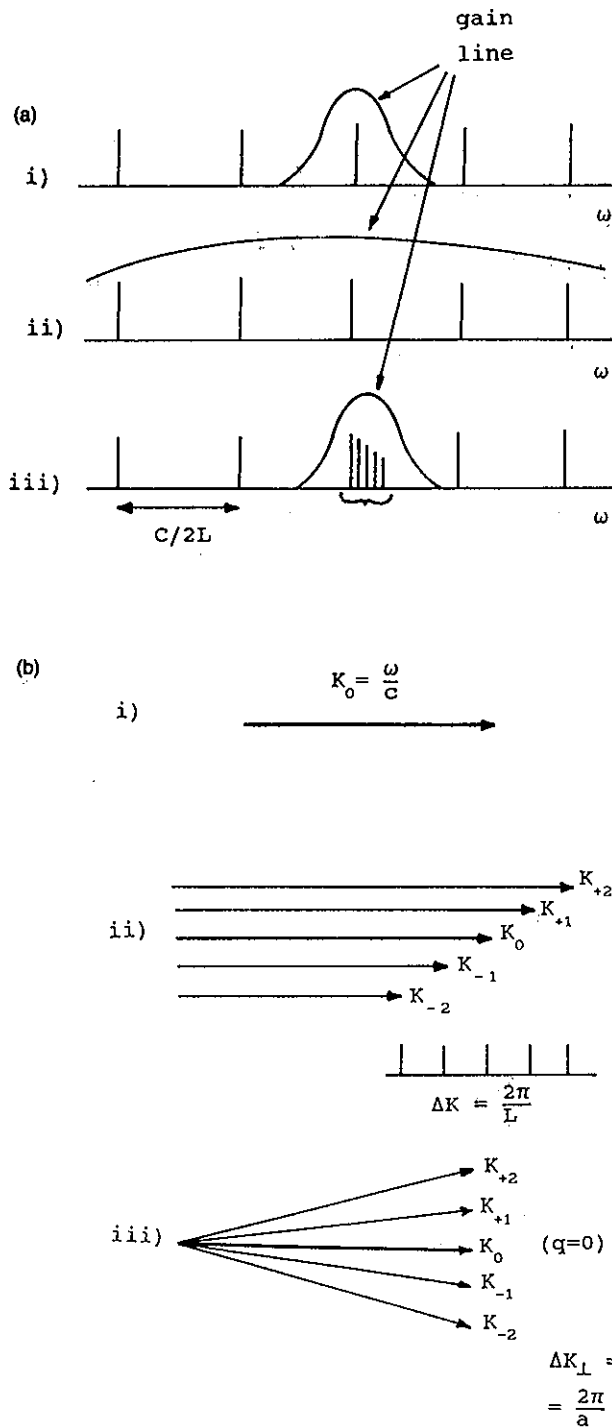


FIG. 1. The ω -space (a) and k -space (b) pictures of the lasing modes in the (i) (1 + 0), (ii) (1 + 1), and (iii) (1 + 2)-dimensional cases.

sional. The resulting ODE replacing the wave PDE has to be coupled to the matter equations giving the evolution of P . In the simple case of a cavity mode resonant with the atomic line, we obtain the so-called Maxwell-Bloch equations. These are three equations coupling field amplitude E of the single mode with the projection onto the same plane wave of the induced polarization $P(r,t)$ and with the local population inversion $N(r,t)$. In fact the three E , P , and N equations may have drastically different damping rates

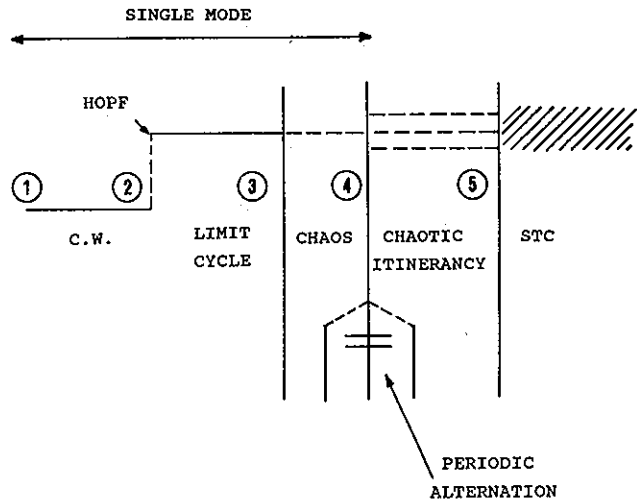


FIG. 2. Space-time complexity in optics. Indication of different behaviors observed in laboratory experiments and in numerical solutions of model equations.

so that the asymptotic dynamics may be ruled by the slower variables. When both P and N are "fast," the dynamics is ruled by a single E equation; when only P is "fast," we have two coupled rate equations for E and N , and when all decay rates are of the same order we must account for the full Maxwell-Bloch equations. We have thus found it useful to classify lasers into three dynamic classes, A, B, and C.⁶

A comprehensive review of experiment and theory for these single-domain, (1 + 0)-dimensional systems is given in the book cited in Ref. 6, covering the period 1982-87 over which these space invariant instabilities have been studied. The terminology (1 + 0), (1 + 1), (1 + 2) refers to the time-space dimensions of the dynamics.

B. (1 + 1)-dimensional optics

Take an optical cavity thin enough to reject off-axis modes, but fed by a gain line wide enough to overlap many longitudinal modes. The superposition of many longitudinal modes means that one must retain the z gradient. Thus the wave equation reduces to

$$(\partial_t + c\partial_z)E = GP, \tag{4}$$

where G is a scaled coupling constant.

Having a PDE, any mode expansion with reasonable wave-number cutoffs provides a large number of coupled ODEs, thus it is immaterial whether P and N are adiabatically eliminated, as in class A and B lasers, or whether they keep their dynamical character as in the class C laser. Anyway, we have enough equations to see space-time chaos.

Equations such as (4) have been solved numerically in the sixties, to explain space variations on a length scale much smaller than L , as seen in regular or erratic mode locking. Figure 2 collects a sequence of possible behaviors as one increases an intensive control parameter (the pump to loss ratio) for a cavity long enough to provide a high

ratio of gain linewidth to free spectral range, or alternatively, as one increases an extensive parameter, that is, the latter ratio for a fixed pump-to-loss ratio. Since the free spectral range is given by $c/2L$, increasing the extensive parameter amounts to increasing the cavity length L .

The circled numbers 1 to 5 denote the transition points.

Threshold No. 1 is the usual laser threshold, whereby uncorrelated spontaneous emission self-organizes into single mode coherent laser action. Mathematically it is a pitchfork bifurcation, with critical divergence of the fluctuation amplitude and correlation time (critical slowing down). These transition phenomena have been experimentally demonstrated in the middle sixties.⁷

In order to consider space variations, one must couple Eq. (4) with the matter equations. This was done by a mode expansion of Eq. (4), and a second threshold, No. 2, which is a Hopf bifurcation toward an oscillatory regime, was introduced.⁸

A third threshold marks the onset of deterministic chaos in a single mode laser. In fact it is a cascade of bifurcations depending on the specific route to chaos, which is influenced by possible laboratory perturbations, as modulations or feedback. The isomorphism of the single mode laser equations with Lorenz equations was first pointed out by Haken.⁹ After that, a large amount of experimental and theoretical investigation has been devoted to chaos in a single mode laser.⁶

Recent consideration of a space-extended (1 + 1)-dimensional optical system by a model made up of Eq. (4) plus material equations has shown evidence of a further behavior, called "chaotic itinerancy."¹⁰ It consists in the jump from one slow manifold to another, i.e., from one quasi-attractor to another. At any time, a single mode with a chaotic behavior is present, but after a while it is replaced by another mode, and so on. Alternatively, in Sec. VI we will show experimental evidence of a nonchaotic, but periodic alternation of modes, indicated in the lower part of Fig. 2. The main indicator of chaotic itinerancy is that, while a local measurement provides a chaotic signal, measurement of the space correlations provides a highly correlated signal.

Above the threshold No. 5 we enter a new regime, called spatio-temporal chaos (STC) where a large number of modes coexist. This regime has been characterized on very general grounds by Hohenberg and Shraiman.¹¹ STC is characterized by some statistical features observed in the experiment reported in Sec. VI. Such features however play no role in the scope of this paper and will not be covered here.

C. (1+2)-dimensional optics

As shown in Fig. 1(iii), let us consider a gain line allowing for a single longitudinal mode, but take a Fresnel number high enough to allow for many transverse modes.

We rescale the transverse coordinates x, y with respect to the cross cavity size a , and the time t to the longitudinal photon lifetime $L/(cT)$, where T is the mirror transmissivity. The new variables are

$$x' = \frac{x}{a}, \quad y' = \frac{y}{a}, \quad t' = \frac{t}{L/cT}.$$

Furthermore we neglect the longitudinal gradient. Then the wave equation reduces to

$$(\partial_t - i\alpha\nabla_1^2)E = GP \quad (5)$$

where ∇_1^2 is the transverse Laplacian and

$$\alpha = 1/4\pi FT.$$

As in the (1 + 1) case, Eq. (5) must be coupled with the material equation. If P has a fast relaxation toward a local equilibrium with the field, and if we expand its dependence to the lowest orders, we have a relation as

$$P = aE - b|E|^2E.$$

Introducing this into Eq. (5), one has a nonlinear Schrödinger equation (NLS) which has been recently considered in many theoretical investigations.¹²

On the other hand, important considerations have been developed for the complex Ginzburg-Landau equation (CGL).¹³ This can be written as

$$\partial_t u = (\alpha_1 + i\alpha_2)\nabla^2 u - \mu u - (1 - i\beta)|u|^2 u. \quad (6)$$

The CGL includes NLS (for $\alpha_1 = 0$) the chemical reaction-diffusion equation (for $\alpha_2 = 0$) and the single mode laser equation (for $\alpha_1 = \alpha_2 = 0$). Otsuka and Ikeda¹³ used a discretized version of CGL on $N = 5$ sites with a space coupling which mimics the second derivative, i.e.,

$$\nabla^2 u \rightarrow u_{i+1} + u_{i-1} - 2u_i \quad (i=1, \dots, N),$$

and gave solutions for $\mu = 1$, $\alpha_1 = \alpha_2 = 0.1$, and β increasing for 10 to 30.

For increasing β the system displays a variety of dynamical behaviors as shown in Fig. 2.

III. DECAY OUT OF UNSTABLE STATES

The transition of a laser from below to above threshold can be accurately traced by control of the gain or losses and measurements of the photon statistics of the output light.⁷ This stationary problem has no connection with Kramers' problem in so far as it consists in measuring the fluctuations around the fixed point, with a particular care in the threshold region which corresponds to a bifurcation. Kramers-like situations occur in optical bistable devices.¹⁴

Here we rather address the problem of the transient decay out of an unstable fixed point toward a stable one. The initial idea¹⁵ was to suddenly change the loss value of a laser cavity (so called Q -switching) in order to instantly bring a laser from below to above threshold. The result can be qualitatively described with reference to Fig. 3. The system parameter (the cavity photon number n) is initially prepared in a stable potential minimum $V_1(n)$ around $n = 0$. At $t = 0$ the potential is switched to $V_2(n)$ which as a maximum at $n = 0$ and a minimum at $n_1 > 0$. The photon number $n(t)$ evolves from the initial distribution $p(n, 0)$ sketched in Fig. 3(b), toward a narrow asymptotic distribution confined around n_1 . The experiment¹⁵ was performed by measuring the instantaneous distribution $p(n, t)$

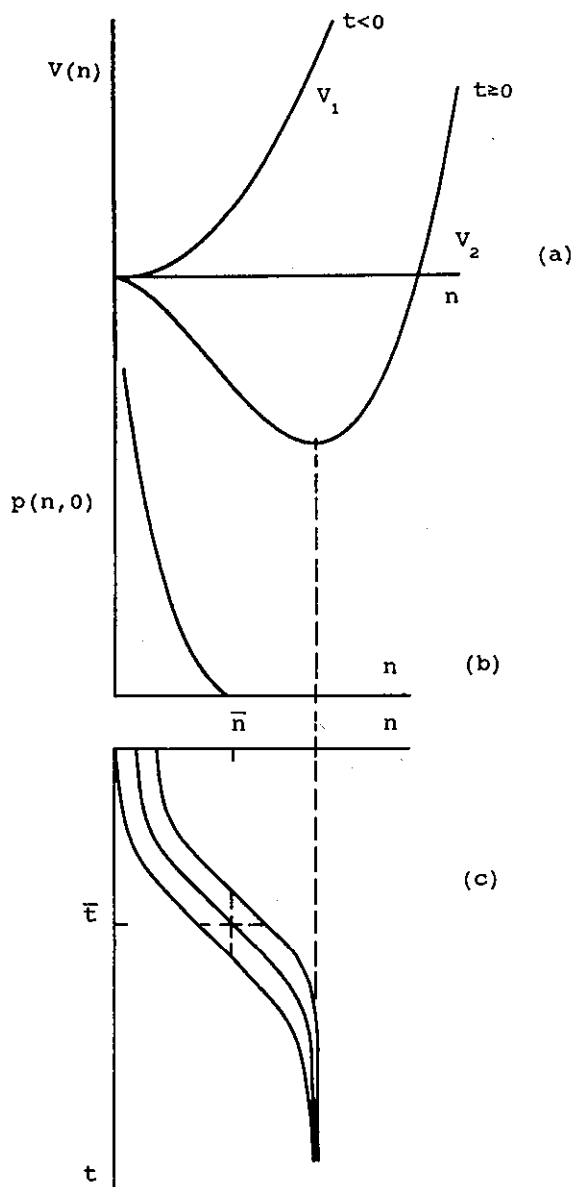
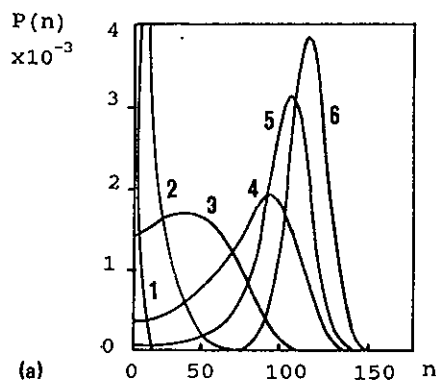


FIG. 3. Transient macroscopic dynamics for the photon number n . (a) Instant switch of the energy potential from $V_1(t < 0)$ to $V_2(t \geq 0)$; (b) initial photon distribution $p(n, 0)$; (c) time evolution of three individual samples $n(t)$ starting from different initial conditions $n(0)$. At a time threshold \bar{t} one measures a photon spread $p(n, \bar{t})$; at a photon threshold \bar{n} one measures a time spread $p(t, \bar{n})$.

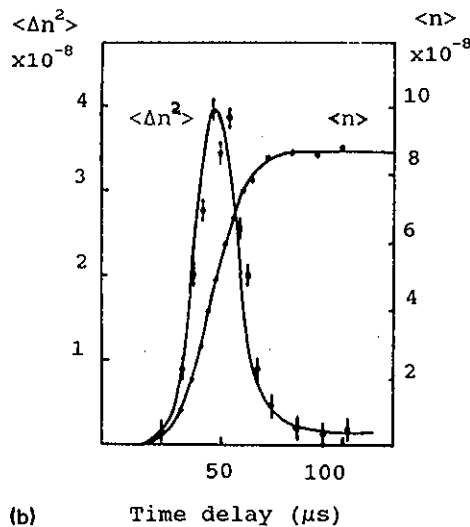
at different delay times starting from $t = 0$ and plotting the corresponding first and second moments (Fig. 4).

It was evident by the appearance of a large peak in the variance of the transient photon number distribution. This fact was explained in terms of an approximately deterministic decay out of a macroscopic unstable state, to be averaged over the statistical distribution of the initial states. Such behavior was later shown to be peculiar of quenching phenomena in macroscopic systems, such as spinodal decomposition in thermodynamic systems.¹⁶

As stressed by Haake,¹⁷ the phenomenon is the transient counterpart of the stationary fluctuations at the critical point of a thermodynamic phase transition (or more



(a)



(b)

FIG. 4. (a) Experimental statistical photon distributions with increasing time delays from 1 to 6 (1 is the initial distribution, 6 is the asymptotic one); (b) evolution of the mean number $\langle n \rangle$ and variance $\langle \Delta n^2 \rangle$ as a function of the delay.

generally at the bifurcation points in a nonlinear dynamics which display the same formal features of a second-order phase transition). Precisely, if we call N the number of degrees of freedom of a macroscopic system decaying out of an unstable state, the initial fluctuations are of the order of $1/N$ [$O(1/N)$], however, in the linear part of the decay they are amplified by $O(N)$, hence the relative fluctuations are of $O(1)$.

The assumption of deterministic evolution out of a spread initial state neglected the role of fluctuations along the build up with respect to the initial ones. The relations between the two types of noise were discussed at the XVII Solvay Conference on Physics.⁷

The quest for discrimination between fluctuations on the initial condition and those along the path led to a new observation method, based on the statistics of passage times at a given threshold.¹⁸ This can be described with reference to Fig. 3(c). If we compare different evolving

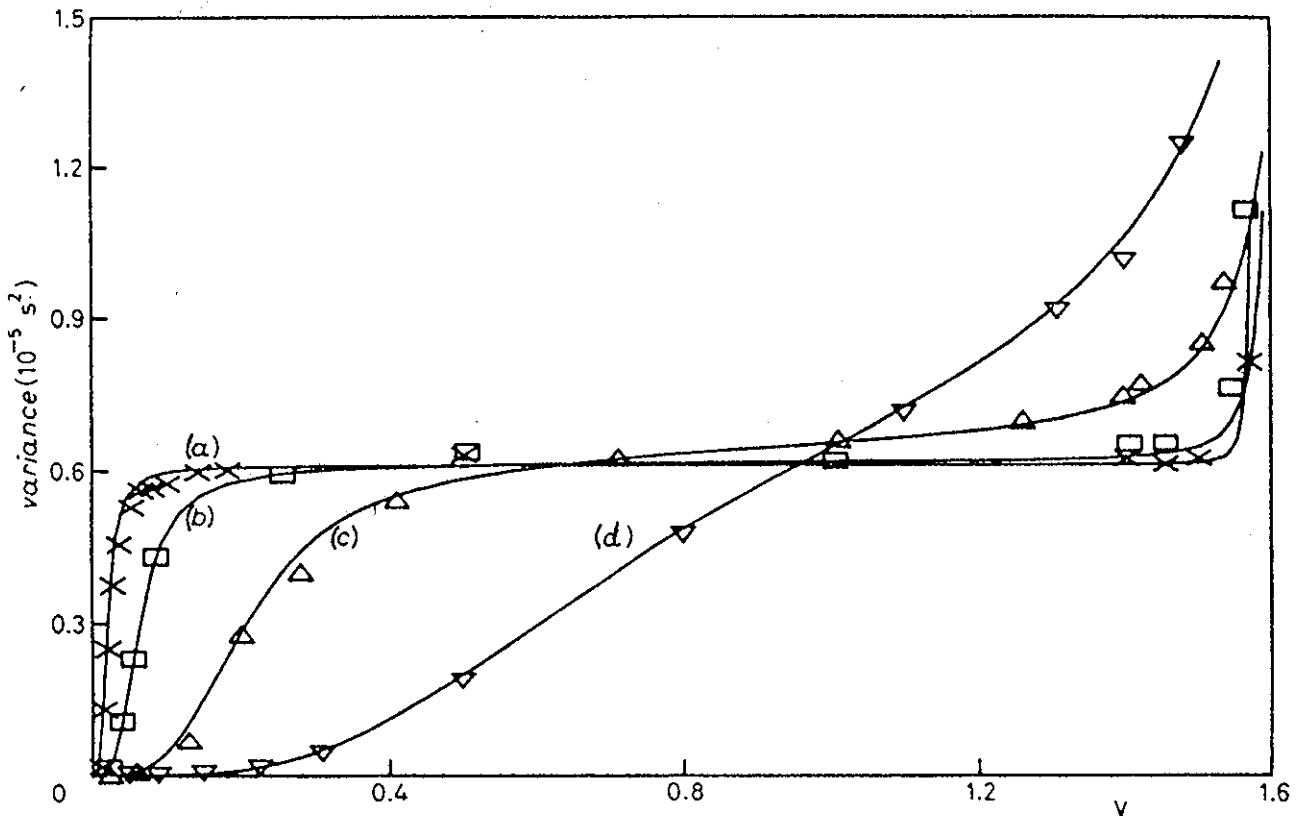


FIG. 5. Experiment of transient decay in a nonlinear oscillator. Variance in the passage times versus threshold V for increasing amounts of applied noise [from (a) to (d)]. The widths of the flat regions correspond to the deterministic amplification regimes where noise can be neglected [from Ref. 18(b)].

paths $n(t)$ out of the same initial macroscopic state, each one of them starts from a different initial condition, sorted from the statistical distribution $p(n,0)$. The photon statistics $p(n,\bar{t})$ (see, e.g., one of those reported in Fig. 4) is measured by setting the delay at \bar{t} and tracing the photon number variations from sample to sample. On the contrary, setting a photon number threshold at \bar{n} we can investigate the spread in passage times through that threshold.

Calibrating the method with an electronic oscillator^{18(b)} we see that for low external noise the variance $\langle \Delta t^2 \rangle$ in the passage times, plotted versus the threshold, is almost constant [Fig. 5(a)], meaning that different paths $n(t)$ are shifted versions of one another, that is, the time jitter between different paths remains constant along the evolution of each path. When instead the external noise is increased (Fig. 5 curve d), fluctuations along the path yield a variance changing from point to point.

From this method it resulted clearly that, when a laser is suddenly switched far above threshold, the fluctuations are mainly due to the initial spread, as already guessed in Ref. 15. The passage time method evidenced an important difference between gas and dye lasers, since in the latter case it permitted detection of the role of pump fluctuations as "noise along the path."¹⁹ It was also applied to semiconductor lasers.²⁰

Both He-Ne and dye lasers have in common a population decay rate that is large with respect to the photon

decay rate (so-called class-A lasers).⁶ Hence the population adiabatically follows the intensity changes, with a consequent reduction of inversion as the cavity losses are lowered. This adiabatic following forbids any overshoot in the laser intensity. Indeed, Q switching in class-A lasers is characterized by an intensity monotonically increasing up to an asymptotic value as in Fig. 4(b). In contrast, when the population decay is lower than the photon decay (class-B lasers) the initially large population storage provides a large intensity pulse by stimulated emission, and only later the population feels the slower depletion channels (either spontaneous emission in ruby and semiconductors, or collisional de-excitations in CO_2). This explains why, after a sudden loss reduction, class-B lasers release giant intensity pulses well above the asymptotic value, whereas class-A lasers do not.

Passage time statistics in a transient CO_2 laser acts as a sensitive detector of the initial photon number which triggers the amplification cascade (so-called statistical microscope²¹). Indeed it can be shown that the second moment $\overline{\delta t}$ of the observed statistics is proportional to the amplification rate, while the first moment \bar{t} provides the average passage time to a given macroscopic photon number n , which can be measured with high accuracy by current detectors. Thus, besides some minor corrections, one has²¹ $n_0 = ne^{-\bar{t}/\delta t}$. Furthermore, the higher-order cumulants of the time statistics provide the error bars of the experimental points. This way one can detect a few initial

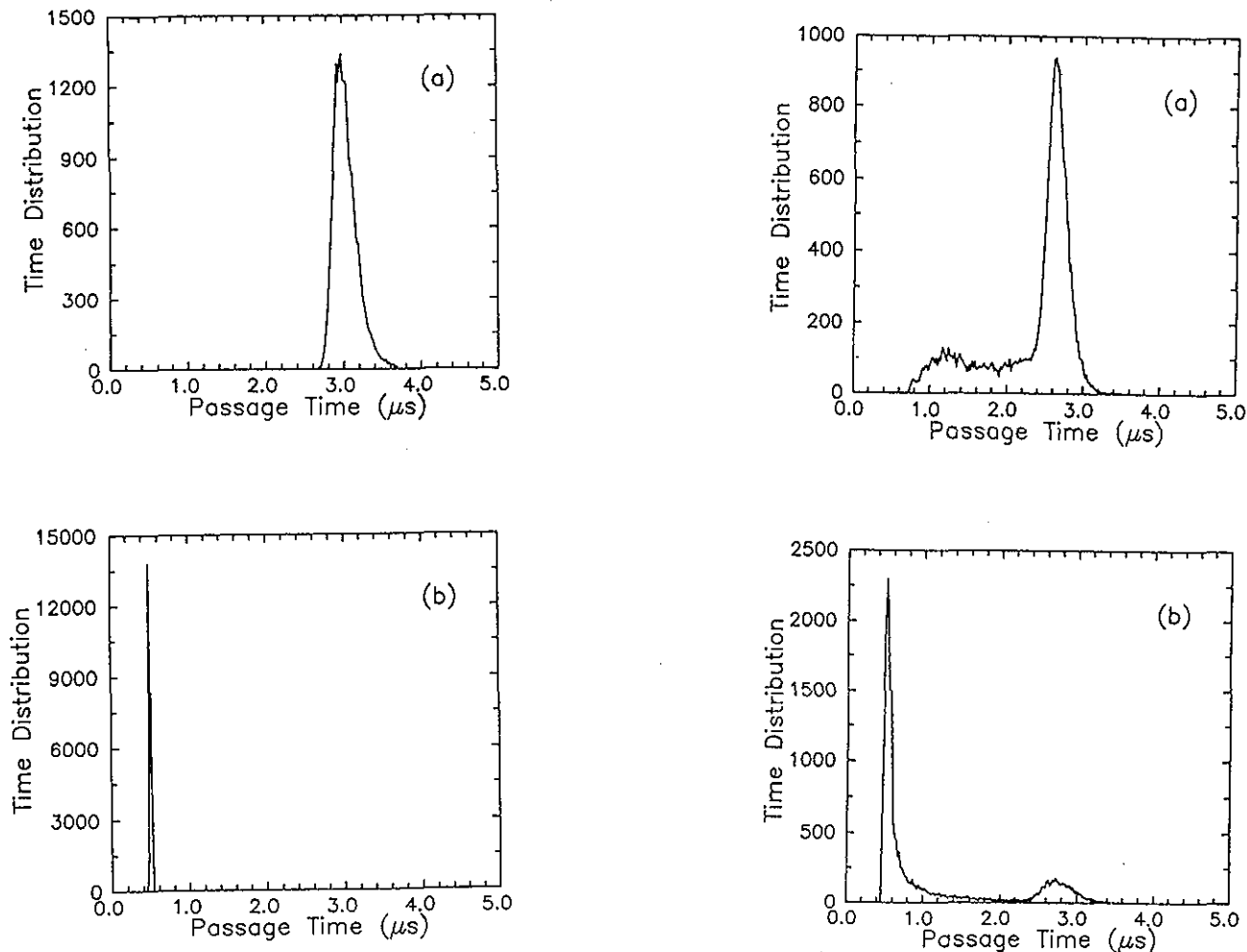


FIG. 6. Experimental passage time distributions from an initial state (from Ref. 53). Left: below threshold (a), and above threshold (b). Right: two-peaked distributions close to threshold.

photons in a laser cavity by linear optical amplification. The reported amplification factors are of the order of 10^8 , but in principle they could be larger. The linearity of the amplification process is preserved up to the saturation photon number, which is over 11 decades in our case.

Recently, experimental evidence of two-peaked transient times statistics was explained as due to population inversion fluctuations.²² When the initial state is very close to threshold, two-peaked distributions of the passage time are observed as shown in Fig. 6. This can be understood as a mixed feature of the laser starting either from below or above threshold. This sensitivity to net gain is peculiar to a class B laser such as the CO₂ laser. Indeed this has a large difference among the photon confinement time (less than 10^{-7} s) the transient build up time (a few microseconds) and the population decay time (a tenth of a millisecond). In the preparation process, each sample of the statistical ensemble adjusts not only to a different photon number, but also to a different gain value, which then is kept constant along the transient evolution because of the class B character. Therefore the field equation has not only an additive noise arising from spontaneous emission but also a multiplicative one due to a variable gain coefficient. This

model with two noise contributions yields theoretical results in agreement with the experiment.

IV. CHAOS WITH MANY ATTRACTORS: NOISE-INDUCED JUMPS AND CRISES

A. Noise-induced jumps and $1/f$ spectra

A class B laser reaches chaos²³ by loss modulation at a frequency close to a nonlinear resonance intrinsic of the system (around 60 kHz for a CO₂ laser).

For a particular parameter window a new robust feature appears, namely the coexistence of two independent stable attractors, one of period $4(f/4)$ and the other of period $3(f/3)$ (Fig. 7). This bistable situation has nothing to do with the common optical bistability where two stable output values appear for a single driving amplitude. We call this coexistence of two attractors "generalized bistability." The left part of Fig. 7 shows the two power spectra of the output intensity, and the right one the phase space projections on the plane (\dot{n}, n) , n being the photon number and \dot{n} its time derivative. Having two stable attractors, a generic initial condition leads to either one, yielding the associated power spectrum. In order to obtain both spectra

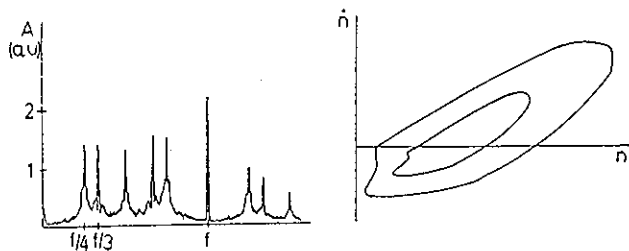


FIG. 7. Modulated CO₂ laser: power spectra and phase portrait (\dot{n}, n) where n is the photon number. $f = 63.85$ kHz. Experimental evidence of generalized multistability (coexistence of two independent attractors). The power spectrum shows that the attractors correspond to $f/3$ and $f/4$ subharmonic bifurcations, respectively; in phase space we see independent loops. The multiple winding (corresponding to period 3 and 4, respectively) is masked by the particular projection.

and phase portraits we switch *on* and *off* the laser system, restarting each time from initial conditions statistically distributed over the two basins of attraction. The high-frequency spectrum around $f = 60$ kHz decays rapidly at low frequencies. Indeed in the few Hertz regime we have only some disturbance due to the 50 Hz electricity supply (dashed line in Fig. 8). Addition of a small amount of noise induces jumps between the two attractors and a corresponding low-frequency jump spectrum (thick line of Fig. 8). Around 10 Hz the new spectral amplitude is more than 20 dB above the noiseless one. This low-frequency spectrum has a power law behavior $f^{-\alpha}$ with $\alpha \sim 0.6$.

The above experiment shows that $1/f$ type low-frequency spectra, that is, power spectra as $f^{-\alpha}$ ($\alpha = 0.6-1.2$), appear whenever there are at least two basins of attraction, and some random noise triggers jumps between them.

Previously, in the study of chaos in an electronic circuit, it was shown²⁴ that in a nonlinear dynamical system with more than one attractor, introduction of random noise induces a hopping between different basins of attraction, giving rise to a low-frequency spectral divergence, resembling the $1/f$ noise well known in many areas of physics. Such an effect was later confirmed by the laser experiment implying two coexisting attractors²³ and in other areas as, e.g., Josephson tunnel junctions.²⁵

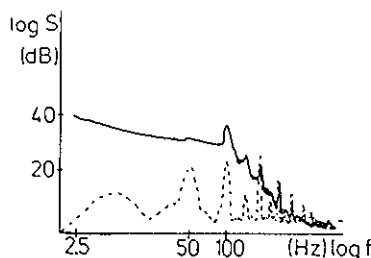


FIG. 8. Experimental power spectra in the case of two attractors, without noise (dashed line), and with noise (solid line). Notice that this low-frequency range is two decades below the high-frequency spectra of Fig. 3. The solid spectrum (noise activated) shows a power law component from 20 to 40 dB above the dashed (jump-free) spectrum.

The relevance of the effect was questioned with two objections:

(a) A noise-induced jump across a boundary leads to a telegraph signal with an exponential correlation and hence a single Lorentzian spectrum.^{26a}

(b) A computer simulation on a nonlinear oscillator yielded a power law only over a limited spectral range.^{26b}

The questions were answered²⁶ with a statement of the empirical conditions under which the $1/f$ spectra appeared, namely: (i) coexistence of at least two attractors, (ii) presence of noise, and (iii) some "weak stability" in the attractors.

As a matter of fact this third condition was rather vague. While question (b) above can be answered criticizing the limited extension of the scanned parameter window which might overlook more interesting behaviors, question (a) introduces a logical dilemma, namely since noise activation across a boundary leads to a Lorentzian spectrum (asymptotic tail f^{-2}) how can one justify an exponent $\alpha < 2$? About the same time, a model of random-random walk in ordinary space, as diffusion in a disordered lattice, showed $1/f$ spectrum²⁷ thus hinting at the necessity of a double randomness to build a non-Lorentzian spectrum. Hence the answer to question a) was in (iii), provided the weak stability of an attractor implies a second randomness.

In the meantime, the amount of stability of an attractor had been quantified by the new concept of crisis.²⁸ Broadly speaking a crisis occurs whenever, by changing a control parameter, the attractor hits its basin boundary, thus merging into the neighbor one.

The weak stability requirement of the laser²³ and electronic²⁴ experiments suggests that we explore the pre-crisis parameter region. To make these concepts more precise, two theoretical models were explored, namely, a one-dimensional cubic iteration map with noise²⁹ and a forced Duffing equation with noise.^{30,31} We recall that a one-dimensional iteration map on the interval has a number of independent attractors equal to the number of extrema. Thus the cubic map can have two attractors and we adjust the parameter range to have two coexisting period-3 orbits. In the case of the Duffing oscillator we explore parameter regions allowing for a large number of coexisting attractors (up to seven). Assume that in both cases we are before crisis and we apply noise. Any indicator of a noise-induced crisis is the mean escape time T from the attractor. Such an indicator has been proved³⁰ to depend on the noise amplitude σ and on the parameter distance ϵ from crisis through a universal scaling law as:

$$T = \sigma^\alpha F(\epsilon/\sigma^\beta). \quad (7)$$

For the case of the logistic map the exponents are³⁰ $\alpha = -1/2$ and $\beta = 1$. Quite below the crisis, for $\epsilon \gg \sigma$, the main dependence of T on the noise amplitude is an exponential one

$$T \sim (\epsilon^{3/2}/\sigma^2) e^{\epsilon^2/2\sigma^2} \quad (7')$$

similar to Kramers diffusion law.²

Very recently there has been a theoretical³² and experimental³³ reconsideration of these scaling laws for noise-induced crises.

Still, an average escape rate as the reciprocal of (7) is compatible with a single exponential decay (Lorentzian spectrum), and numerical simulations provide power law fits with different α exponents, depending on the accuracy of the fit and the width of the frequency window over which the fit is performed, thus the question of whether the above laboratory and computer experiments deal with one, or a few, decay rates, or with a large hierarchy of decays organized along specific rules, is not yet solved.

On the other hand, a common approach to the $1/f$ problem is based on the composition of a large number of Lorentzians whose weights are log-normally distributed,³⁴ thus fulfilling the relation

$$\int_{\gamma_1}^{\gamma_2} \frac{\gamma}{\omega^2 + \gamma^2} p(\gamma) d\gamma \approx \text{const} \times \frac{1}{\omega} \quad (8)$$

provided $p(\gamma) \sim 1/\gamma$, and for the frequency range $\gamma_1 \ll \omega \ll \gamma_2$.

In the quest for the second randomness postulated in Ref. 27, the initial tentative was to look for a large number of attractors coupled by a set of kinetic equations describing the transition rates across their boundaries. In Eq. (8) it is not enough to have many Lorentzians, but they must be summed up with the right weights. As shown in Ref. 35 on very general grounds, a log-normal distribution is equivalent to a cascade of processes and hence it implies a double randomness.

Now, the numerical evaluation of Ref. 31 showed that for some control parameters the boundary between basins of attraction was an intricate set of points, through which it was impossible to draw a simple line. In such cases the noise was most effective in yielding low-frequency $1/f$ -like spectra. In the meantime, the fractal structure of a basin boundary for chaotic dynamics was investigated.³⁶

The self-similar structure of a fractal boundary between two attractors seemed the key for the second randomness, more plausibly than a clustering of many attractors. Thus, we conjectured that the boundary structure was really responsible for a large number of decay constants log-normally distributed.

The conjecture can be tested by an elementary model for the motion of the phase point within a fractal basin boundary in the presence of random noise.³⁷ The boundary region of two basins of attraction A and B is modeled as two adjacent one-dimensional lattices of sites. Suppose we start from site i . At each discrete time step, if i belongs to A ($i = i_A$) it moves one step forward on the same lattice [$i_A \rightarrow (i_A + 1)$] and if it belongs to B it goes one step backward [$i_B \rightarrow (i_B - 1)$]. In the absence of noise, once the motion has started on one basin, it will remain on it forever. In the presence of noise, at each time step there is a finite probability of a "cross" jump at the same lattice site, from stripe A to B : $i_A \rightarrow i_B$. Now the second randomness comes into play. The separation between stripes A and B varies from site to site according to a fractal distribution, which however is truncated. Normalizing to 1 the maximum sep-

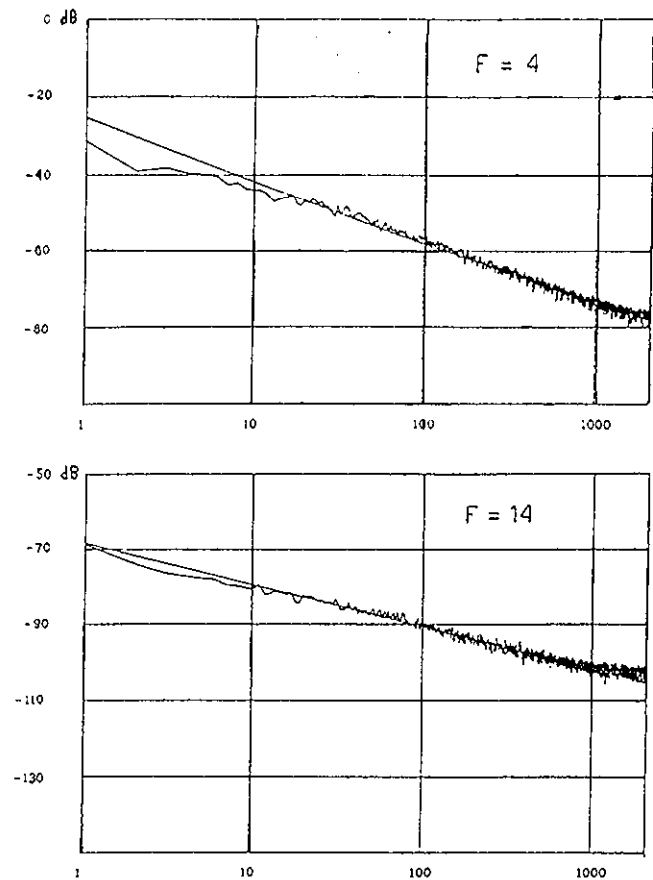


FIG. 9. Deterministic motion on two one dimensional lattices with random mutual separations and each site, at with possible noise induced jumps. Power spectra (vertical) versus frequency (horizontal) in log-log scale. Wavy lines: measured spectra, straight lines: best fits, whose slopes α are 1.7 ($F = 4$), and 1.1 ($F = 14$).

aration, $A-B$, at each site we sort one separation from the set $2^{-1}, 2^{-2}, \dots, 2^{-F}$; F is the truncation of the fractal process. Evolving the model with added noise and fractal separation between the two attractors, one can measure the correlation function on the time-dependent position.

In Fig. 9 we show two power spectra for $F = 4$ and 14, respectively. As the fractality increases, the slope of the log-log plot goes from about 2 (single Lorentzian) to about 1 ($1/f$ spectrum). The Lorentzian ($\alpha = 2$) of the random telegraph model is easily recovered for $F = 1$, thus showing that noise-induced jumps across a regular line boundary fulfill the intuitive expectation of a single decay rate. An analogy with the random-random walk is easily drawn. Indeed the motion describes above has an rms deviation from the average which changes from about \sqrt{t} to $|\log t|^2$ as the fractality F increases from 4 to 14, and the two trends are associated respectively with a Lorentzian and a $1/f$ spectrum.²⁷

The recently introduced phenomenon of self-organized criticality has received much attention.³⁸ Self-organized criticality applies to spatially extended dynamical systems, wherein the dynamics cannot be reduced to a few degrees of freedom. After some initial transient period, these systems settle down to a steady state whose statistics are de-

scribed by power law distributions, in both space and time, reminiscent of critical phenomena familiar from second-order phase transitions. Unlike these equilibrium phenomena, however, the critical state is achieved without the necessity of tuning a control parameter. Instead, the system naturally evolves in the critical state; moreover, changes of parameter induce a collective readjustment among the degrees of freedom that maintain the critical state. Our present understanding of self-organized criticality is drawn largely from numerical simulations on cellular automata.

This subsection was instead devoted to low-dimensional dynamical systems without extension, and the $1/f$ character emerged from the extended structure of the phase space where the attractors are embedded. Whether this phenomenon and self-organized criticality have anything in common is an open question.

B. Spontaneous interattractor transitions (crises)

In nonlinear dynamics it is generally possible to have collisions between unstable orbits and chaotic attractors, leading to interior, boundary, and external crises.^{28,39} The former one preserves the chaotic attractor monotonically enlarging its basin, the second one destroys the attractor by sweeping off its basin of attraction, while the latter one discontinuously enlarges its basin of attraction. The presence of those different crises in the system depend on the amount of dissipation.³⁹ Such crises have been experimentally observed in a variety of systems.⁴⁰ Boundary crises in the modulated laser have been observed by Glorieux *et al.*⁴¹

Working on the modulated CO₂ laser we have given experimental evidence of the three types of crises which are due to collisions among strange attractors and unstable periodic orbits created in saddle node bifurcations.⁴² These collisions are also responsible for the existence of isles that can be reached only by hard mode excitation and for periodic windows that separate different regions.

Furthermore, from the shape and size of the multi-stable region as a function of the modulation amplitude, we draw a connection between the amount of attractor overlap in parameter space and the volume contraction rate in phase space, that is, the dissipativity of the dynamical system.

Presumably these phenomena can be fitted with the zero noise limit of a scaling law such as Eq. (7). Whether these transitions are ruled by a single time constant or by a self-similar $1/f$ type cascade, is still a question to be treated.

V. SHIL'NIKOV CHAOS: HOW TO CHARACTERIZE HOMOCLINIC AND HETEROCLINIC BEHAVIOR BY RETURN TIME MAPS

Shil'nikov dynamics⁴³ corresponds to orbits asymptotic to an unstable saddle focus in at least a 3-D space. Limiting to a 3-D space let us call $\alpha \pm i\omega$ the pair of complex eigenvalues on the stable ($\alpha < 0$) manifold and $\gamma > 0$ the eigenvalue in the unstable direction orthogonal to the plane.

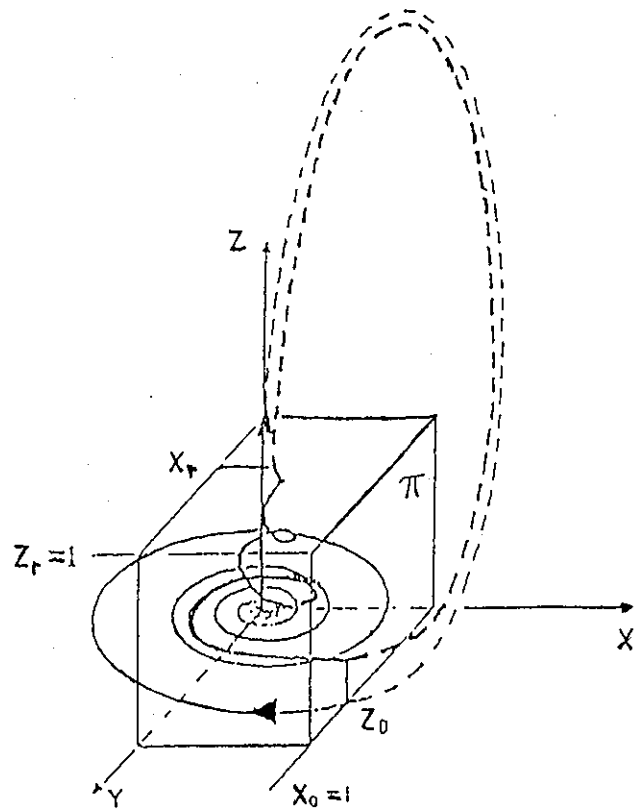


FIG. 10. Schematic representation of a trajectory in Shil'nikov dynamics and construction of unit box leading to the unidimensional map (12) through the linearization of the flow around the saddle focus.

Let us consider a dynamics where all fixed points are unstable, within a given range of control parameters. We call such situation a regime of competing instabilities.⁴⁴ In physical implementations⁴⁵ we can adjust the control parameter in order to isolate a nonzero set of initial conditions such that all trajectories departing from there asymptotically approach the unstable saddle focus and remain at a finite distance from all other fixed points. In such a case, under the Shil'nikov condition

$$|\alpha/\gamma| < 1 \quad (9)$$

the motion becomes chaotic.

Two orbits of this type spiraling around an unstable saddle focus are qualitatively sketched in Fig. 10. With the understanding that the only interesting dynamical features occur around the unstable point we obtain a global description by just studying the linearized dynamics within a small box.

We orient the three axes along the eigenvectors with x - y coinciding with the stable plane and z being the expanding direction. We take the π plane (vertical plane of equation $x = 1$ containing a face of the cube) as the Poincaré section and we calculate the return map for the coordinate z . Starting at $t = 0$ at $z = 0$ on $x = 1$ (y is irrelevant for the following considerations) the phase point leaves the upper cube side $z = 1$ at time τ such that $1 = z_0 e^{\gamma\tau}$, from which it results

$$\tau = - (1/\gamma)\log z_0. \tag{10}$$

The horizontal coordinate x evolves over the same time as

$$x(\tau) = e^{-\alpha\tau} \cos \gamma\tau, \tag{11}$$

since the initial condition is $x(0) = 1$. Neglecting a phase shift due to the y position, we constrain the motion external to the box to a rigid translation $x(\tau) \rightarrow z_1$ (see dashed trajectories). Additionally, an offset ϵ is added at each turn and may be considered as a second control parameter, the first one being the ratio $|\alpha/\gamma|$. Using relation (10) and writing z as z_{n+1} and z_0 as z_n we obtain the return map

$$z_{n+1} = z_n^{\alpha/\gamma} \cos[(\omega/\gamma)\log z_n] + \epsilon, \tag{12}$$

which describes the homoclinic orbits.

The map (12), even though representing a sensible global description, may provide a poor experimental criterion whenever the z coordinates on the π plane are clustered in a small region. A lack of experimental sensitivity appears in experimental return maps which do not display the nice features that Eq. (12) provides for the theory. Such was the case for the Belousov-Zhabotinski reaction.⁴⁶ On the other hand, the above behavior appears rather universal whenever one can isolate a spiral-type orbit, as occurs in Lorentz or Roessler chaos.⁴⁷

In dealing with a quantum optical experiment we introduced a more sensitive dynamical indicator.^{48,49} Based on the logarithmic relation between position z on the π plane and times τ that the orbits take to return to that plane, and assuming that the relevant time is that spent in the box of Fig. 7, Eq. (12) transforms via relation (10) into a return map for orbital times. Rescaling τ as $T = \gamma\tau = -\log z$ one obtains

$$\begin{aligned} T_{n+1} &= -\ln[\exp(-\alpha/\gamma T_n)\cos(\omega/\gamma)T_n + \epsilon] \\ &= -\ln[\phi(T) + \epsilon]. \end{aligned} \tag{13}$$

Comparison of Eqs. (12) and (13) shows the enhanced sensitivity to fluctuations of the T map with respect to the z map. Indeed, suppose that the offset ϵ from homoclinicity is affected by a small amount of noise. The sensitivities of the two maps to such a noise are given, respectively, by $\partial z/\partial \epsilon = 1$ and

$$\frac{\partial T}{\partial \epsilon} = [\phi(T) + \epsilon]^{-1}. \tag{14}$$

This sensitivity factor acts whenever $\phi(T) + \epsilon$ becomes very small. Note that this is not yet deterministic chaos; in fact, large fluctuations can be expected even for a regular dynamics with a fixed point T^* . Note also that it is not associated with the homoclinicity condition $\epsilon = 0$; in fact, for finite ϵ there may be a T^* such that $\phi(T^*) + \epsilon = 0$.

Since a homoclinic orbit is the dynamic counterpart of repeated decays out of an unstable state, the result is like repositioning the initial condition in an experiment on a single decay of the type considered in Sec. III. Here the repetition is automatically provided by the contracting motion asymptotic to the stable manifold. As a consequence,

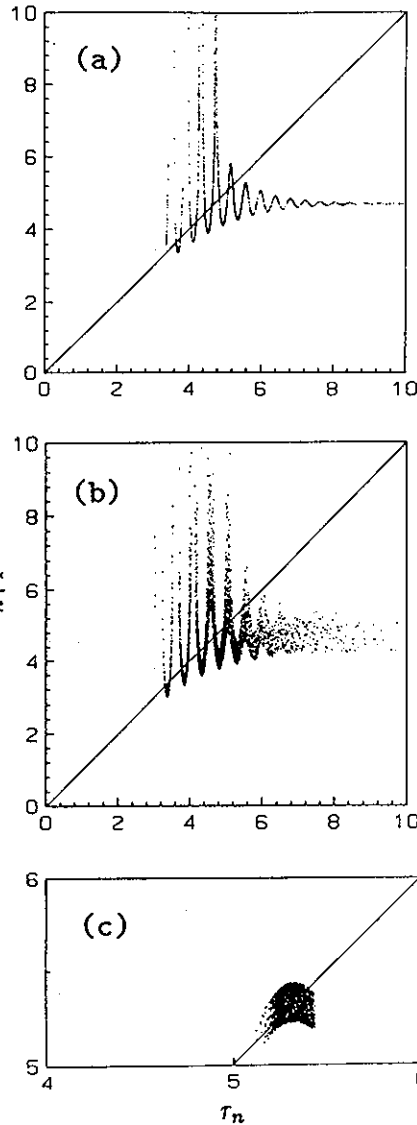


FIG. 11. Numerical iteration maps for return times in Shil'nikov chaos. Parameter values: $\omega/\gamma = 13.0$, $\alpha/\gamma = 0.986$, $\epsilon = 0.01$. (a) and (b), T maps without and with noise $\delta\epsilon = 10^{-2}$, respectively. (c) Stable fixed point of the regular dynamics, broadened by a noise $\delta\epsilon = 10^{-2}$.

superposed upon the deterministic dynamics (either regular or chaotic), the high sensitivity [Eq. (14)] may provide a broadening of the T maps not detectable in the z maps whenever noise in the offset ϵ is present.

In fact, the model description $\dot{x} = F(x)$ of a large system in terms of a low-dimensional dynamic variable x is just an ensemble-averaged description, and residual fluctuations on position x must be considered at some initial time, even though the successive evolution is accounted for by a deterministic law. In our case such a fluctuation is a stochastic spread $\delta\epsilon$ on the offset ϵ of the position z .

As shown in Fig. 11, the same amount of $\delta\epsilon$ in Eqs. (12) and (13) leaves the z maps unaltered, while it strongly affects the T maps. If we specialize the map parameters α , γ , ω , and ϵ to a regular orbit (fixed points both in z and T spaces), introduction of $\delta\epsilon$ does not broaden the

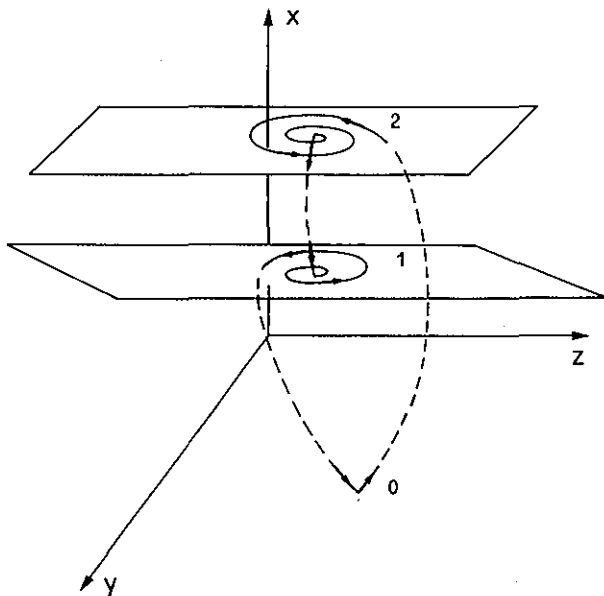


FIG. 12. Schematic view of a trajectory in the phase space when the dynamics is affected by all three unstable stationary points.

z point, while the T point broadens.

For example, the values $\alpha/\gamma = 0.98$, and $\epsilon = 0.01$ yield one fixed point $T^* = 5.327$, with sensitivity $\delta T^*/\delta\epsilon = 182$ [Fig. 11(c)]. Note that the noise effect reported here has nothing to do with additive noise effects on return maps.⁵⁰ Indeed, the latter effects refer to the scaling behavior near stationary bifurcations, whereas our data refer to transient fluctuation enhancement, and they do not leave a permanent mark (such as an orbital shift or broadening).

Thus, while Shil'nikov chaos is a deterministic effect described on an average by the backbone of the z or T maps, the superposed thickening is a noise effect peculiar to T maps undetectable in z maps. This new effect is a specific indicator of intrinsic fluctuations, and it permits a demarcation line to be drawn between a real-life experiment and a model simulation, from which this second feature is absent.

After having summarized the main features of Shil'nikov chaos we describe the corresponding experiments.

The experimental setup consists of a single mode CO₂ laser with a loss modulator driven by a signal proportional to the laser output intensity. Single mode CO₂ laser dynamics is described by two coupled differential equations, for the laser intensity $x(t)$ and the population inversion $y(t)$. The presence of a feedback signal $z(t)$ introduces a third degree of freedom. Such a system is described by three first-order differential equations for $x(t)$, $y(t)$, and $z(t)$. Keeping all other parameters fixed, the dynamics is controlled by varying a bias voltage B in the feedback loop. Figure 12 shows a schematic view of the trajectory in the three-dimensional space, obtained by a linear stability analysis of the motion around the stationary points, plus qualitative connections between the linear manifolds (dashed lines).

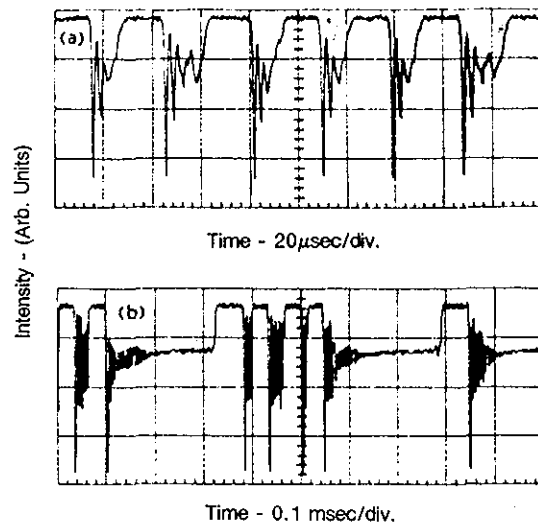


FIG. 13. Time plots of the laser intensity in the regime of Shil'nikov chaos. (a) and (b) refer to two different gains of the feedback loop. (b) shows two long transients corresponding to a large number of small spirals around the saddle focus.

We can visualize $(x-z)$ phase-space projections, by feeding onto a scope the photodetector signal proportional to the laser output intensity $x(t)$ and the feedback voltage $z(t)$. This phase-space projection consists of closed orbits visiting successively the neighborhoods of the three unstable stationary points 0, 1, and 2.

The local chaos around point 1, established at the end of a subharmonic sequence, has been characterized by standard methods such as power spectra and correlation dimension measurements.⁵¹ The competition of the three instabilities in controlling the global features of the motion was described in Ref. 45. Here the control parameters are adjusted in order to have a dominance of the saddle focus, so that the motion consists of a quasi-homoclinic orbit asymptotic to it.

Figure 13 reports experimental plots of the laser intensity versus time for two slightly different conditions. Figure 13(b) shows evidence of a homoclinic orbit in the two long transients, which provide a lengthy permanence in a phase space region of almost constant intensity. This appears more clearly in the corresponding phase space projections [Fig. 14(a) and (b)]. For comparison we give in Fig. 14(c) a photographic exposure (over 1 s) of 30 000 orbits similar to the single one of Fig. 14(a), to show the stability of shape.

The time spacings are measured by setting a threshold circuit near the top of the largest peak of the intensity signal. A time-to-amplitude converter (TAC) yields the sequence T_i of successive time spacings, which is then classified as a statistical distribution by a multichannel pulse height analyzer, or stored in a digitizer, so that correlation functions or iteration maps can be sorted out.

The statistical distribution of return times is a broad featureless curve which does not offer cues on the ordering of T_i . On the contrary, the iteration map (T_{i+1} vs T_i) displays a regular structure [Fig. 15(a)]. To check whether

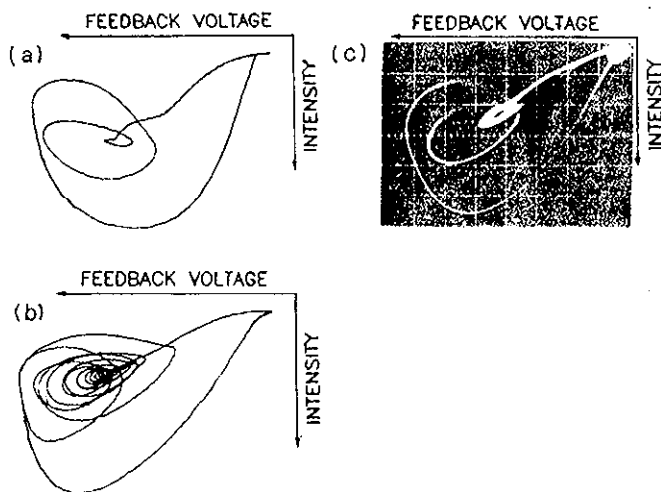


FIG. 14. Phase space projections x - z (laser intensity-feedback voltage). (a) and (b) are single orbits obtained by a digitizer, referring to the same parameters of Figs. 13(a) and (b), respectively, (c) is the superposition of 30 000 orbits of type (a).

we are in the presence of a one-dimensional (1-D) iteration map, and the remaining thickness is due to the observation technique, or the map is more than 1D, we report in Fig. 15(b) the iteration maps corresponding to three regular situations.

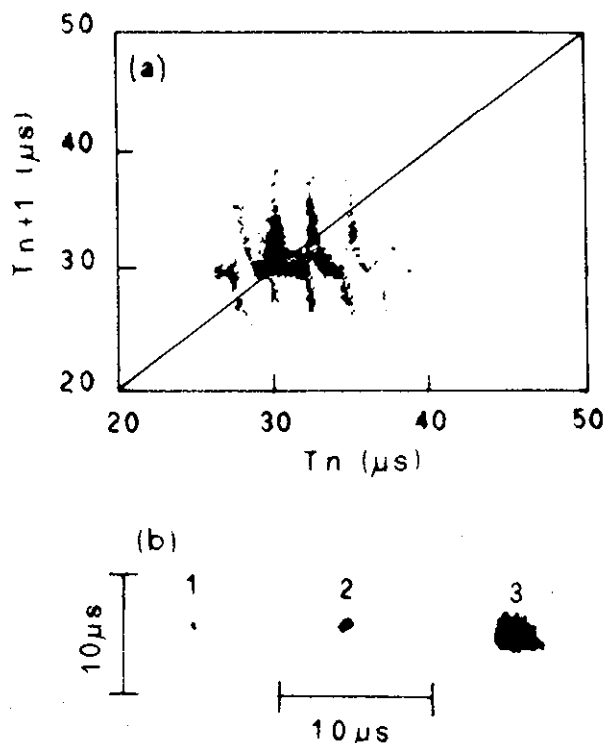


FIG. 15. Experimental iteration maps of the return times: (a) refers to Fig. 13(a); (b) shows the maps corresponding to regular periodic situations, namely, (1) an electronic oscillator, (2) the laser in a regular periodic regime, and (3) the laser just at the onset of the instability but still with a regular period.

In the absence of fluctuations in T_i they should be pointlike (the image of a stable fixed point). In fact, spot 1 of Fig. 15(b) is the calibration with an electronic oscillator and it just shows the resolution of the TAC, spot 2 corresponds to the laser in a regular periodic regime away from the Shil'nikov instability, and spot 3 corresponds to the laser on the verge of the instability but still with a regular period. In this last case, the fluctuation associated with the nearby transition shows that, even without chaos in the return time, the close approach to an instability point introduces a fluctuation enhancement, which has no theoretical counterpart in the current treatment of deterministic chaos. To deal with this broadening, the dynamical equations should include a statistical spread in the injection coordinate at the Poincaré section near the saddle focus, to account for the macroscopic character of the experimental system. As it was shown in Ref. 15, even though this spread has no relevance on the average dynamics, it contributes a large transient fluctuation whenever the system decays from an unstable point.

This suggests a consideration at the borderline between system dynamics and statistical mechanics. Nonlinear chaotic dynamics is described by a small number of coupled equations

$$\dot{x}_i = F_i(\{x_j\}), \tag{15}$$

where $\{x_j\} = x_1, x_2, \dots, x_N$, and $N \geq 3$. In elementary systems as a driven pendulum, x_i are associated with simple variables as momentum, coordinate, and driving amplitude of the pendulum. Whenever the system is a macroscopic one, N is of the order of the Avogadro number, and the reduction to a small number of coupled collective variables implies suitable ensemble averages. If however there are sizable transient fluctuations as described in this section and in Sec. III, then the collective equations are

$$\langle \dot{x}_i \rangle = \langle F_i(\{x_j\}) \rangle. \tag{16}$$

This reduces to a simpler version such as Eq. (15)

$$\langle \dot{x}_i \rangle = F_i(\{\langle x_j \rangle\}),$$

used in models or computer simulations, only whenever

$$\langle \delta x_i^2 \rangle / \langle x_i^2 \rangle \ll 1.$$

Thus the transient fluctuation enhancements associated with escapes from unstable points have to be dealt with by a wise combination of Poincaré and Boltzmann strategies.

VI. CHAOTIC ITINERANCY IN OPTICS

This section reports (1 + 2)-dimensional dynamics in an extended optical medium. By placing a gain medium in a ring cavity, the generated field displays time and space features. The size of a cavity pupil controls the number of transverse modes which can oscillate. Reference 52 reports two different regimes, namely one of a low-dimensional chaos, where a single mode at a time is oscillating, and a small number of modes alternates in a fashion which displays close similarities with the recently introduced concept of "chaotic itinerancy,"¹⁰ and one of space-time chaos

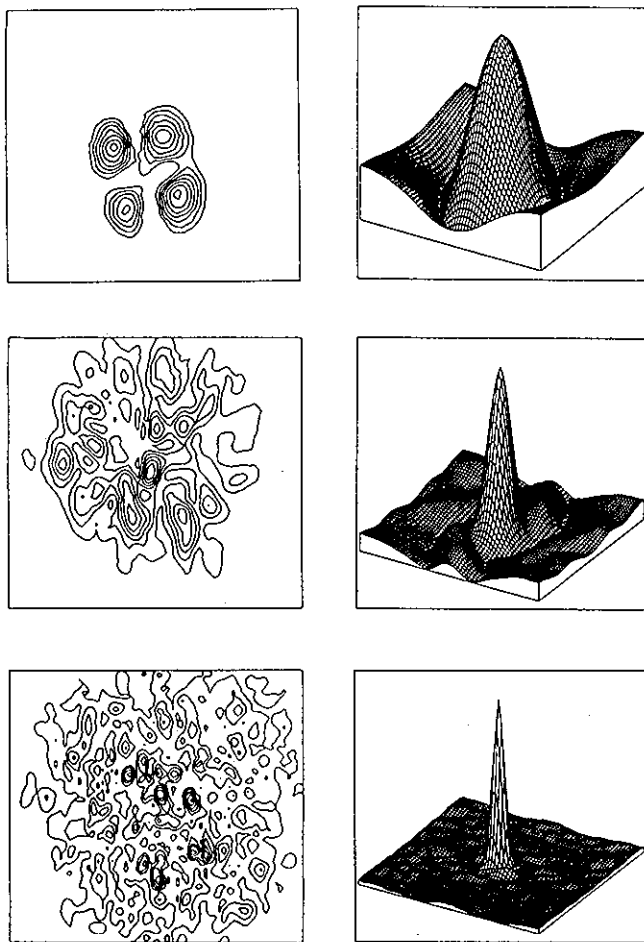


FIG. 16. Intensity distribution on the wavefront (left) and space auto-correlation function (right) for increasing Fresnel number. (a) $F = 5$, one single mode at a time is present, ratio between coherence length ξ and frame size D is $\xi/D \approx 1$; (b) $F = 20$, $\xi/D \approx 0.25$; (c) $F = 70$, $\xi/D \approx 0.1$.

where many modes oscillate simultaneously yielding a very small transverse correlation length and spectral fluctuations with Gaussian statistics, according to Ref. 11.

The experimental setup consists of a ring cavity with photorefractive gain provided by a BSO (bismuth silicon oxide) crystal to which a dc electric field is applied. The crystal is pumped by a cw argon laser.

The Fresnel number of the cavity is controlled by a variable aperture. Here, F can be varied in the range from approximately 0 to 100. This corresponds roughly to the variation of the number of transverse modes that can oscillate. The mechanical and thermal stability are ensured on time intervals longer than those of the measurements (half an hour).

Figure 16 shows the transverse (x, y) intensity pattern recorded by the video camera (left) and its spatial auto-correlation function (right). For low F ($F = 5$) one single mode at a time oscillates and the wavefront is wholly correlated, indeed the correlation length ξ is of the same order as the cross size D of the beam [Fig. 16(a)]. For high F ($F = 70$) many modes oscillate simultaneously, yielding a speckle-like pattern [Fig. 16(c)] whose correlation length

is very small ($\xi/D < 0.1$). The correlation test is crucial, otherwise one might suppose that the intensity pattern at the left refers to a pure mode with a large mode number. Between these two asymptotic limits, we have a smooth variation of the ratio ξ/D , with intermediate situations as shown in Fig. 16(b).

The low F limit corresponds to a periodic alternation of a few modes of the diffraction-limited propagation followed by a dark period. The radial quantum number is always 0 and the azimuthal quantum number changes from $q = 0$ to q around 10. (From now on, we identify the modes by their azimuthal quantum number.

To study the time behavior, the input of an optical fiber picks up the intensity at a generic point on the wavefront (the signal level is a suitable code of each mode). The time plot shows fine details on a time scale of seconds, corresponding to the dielectric relaxation time of BSO. This time scale is typical of the fluctuations in a pure mode and of the intermode switches. Each mode persists for a time of the order of a few minutes. The mode pattern [e.g., 7,6,5,4,3,2 in Fig. 17(b)] repeats almost periodically. To improve the selectivity we commute from the pinhole (low-pass filter) to the pinhole plus an axial stop (band-pass filter). For the same aperture size, introduction of the axial stop cuts off the lowest modes (1 and 0) and produces the regularization shown in going from Fig. 17(a) to Fig. 17(b).

At the minimum Fresnel number for which some signal is observed (F around 2) four different modes still oscillate one at a time, followed by a dark interval, in a very regular periodic sequence. We call such a behavior "periodic alternation." On increasing the pump intensity, the frequency of the alternation increases but it remains regular. For a slight increase of F above 5 the regularity is lost, that is, the duration of each mode is no longer repeatable. This is an experimental evidence of "chaotic itinerancy."

In the high F limit, when $\xi/D \ll 1$, the experiment⁵² shows the connotations of spatiotemporal chaos (STC) consisting¹¹ in a local non-Gaussian statistics and in Gaussian spectral fluctuations.

In conclusion, periodic alternation and STC are two asymptotic limits for very small and large Fresnel numbers in a $(1 + 2)$ -dimensional optical system. At the lower edge of the intermediate region we observe chaotic itinerancy. For still larger F we should expect transition phenomena which are not simply a mathematical bifurcation as the usual laser threshold but which display the scaling properties of phase transitions in extended media.

Recently the role of phase singularities, or topological defects of optical fields, in mediating the transitions (either periodic or chaotic) from one slow manifold to another has been demonstrated experimentally.⁵³ At variance with the material waves which are easily visualized in terms of matter displacements, in the case of an optical field a phase measurement requires heterodyning against an external reference. Phase information is extracted by beating the signal with a reference beam onto a videocamera. When the reference beam and signal beam are parallel, the phase

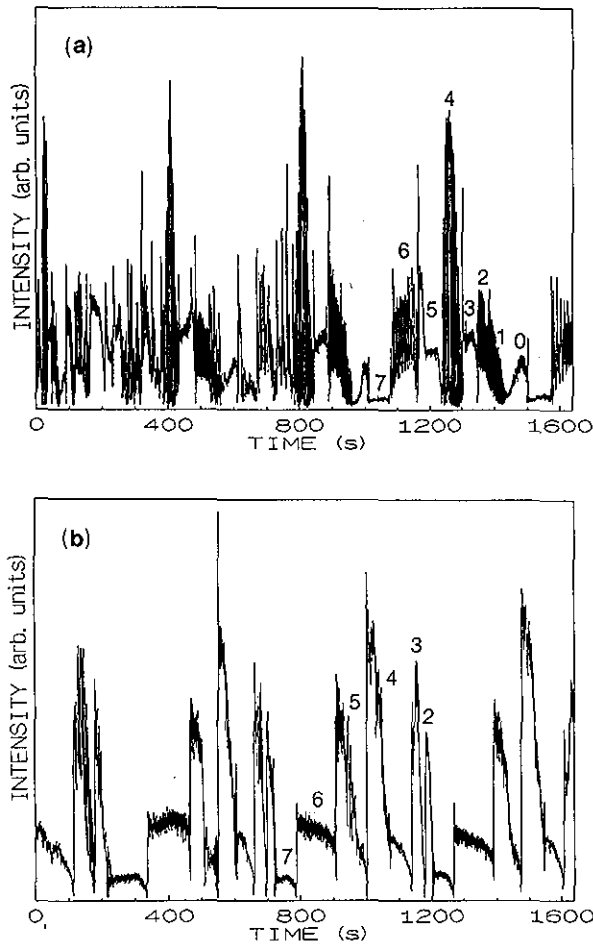


FIG. 17. Time records of the local intensity (samples collected at 10 Hz rate) at $F = 8$: (a) with the low-pass filter (chaotic itinerancy); (b) with the bandpass filter (periodic alternation).

singularity appears as a vortex. A tilting between the two beams transforms the vortex into a dislocation of a fringe lattice, whose period is a function of the tilt angle.

The role of the defect dynamics in controlling the transition rates is the object of current investigation.

¹For early statements of the organization problems see: J. Von Neumann, *Theory of Self-Reproducing Automata*, edited by A. W. Burks (University of Illinois, Urbana, 1966) and H. von Foerster, "On Self-Organizing Systems and their Environments," in *Self-Organizing Systems*, edited by M. C. Yovits and S. Cameron (Pergamon, Oxford, 1960), pp. 31–50; for a seminal model see: A. M. Turing, *Proc. R. Soc. London Ser. B* **237**, 37 (1952).

²H. A. Kramers, *Physica (Utrecht)* **7**, 284 (1940).

³P. Hänggi, P. Talkner, and M. Borkovec, *Rev. Mod. Phys.* **62**, 251 (1990).

⁴*Measures of complexity and Chaos*, edited by N. B. Abraham, A. M. Albano, A. Passamante, and P. E. Rapp (Plenum Press, New York, 1989).

⁵A. L. Schawlow and C. H. Townes, *Phys. Rev.* **112**, 1940 (1958), see in particular the section entitled "Selection of modes for amplification."

⁶By now a classification of laser dynamical types has become of general use, depending on the number of coupled equations which describe the single mode dynamics, namely, Class A, B, C when the number of equations is 1, 2, or 3, respectively. See F. T. Arecchi, in *Instabilities and Chaos in Quantum Optics*, edited by F. T. Arecchi and R. G. Harrison (Springer-Verlag, New York, 1987), p. 9.

⁷F. T. Arecchi, in *Order and Fluctuations in Equilibrium and Nonequilibrium Statistical Mechanics*, XVII International Solvay Conference in

Physics, edited by G. Nicolis, G. G. Dewel, and J. W. Turner (Wiley, New York, 1981), pp. 107–157.

⁸H. Risken and K. Nummedal, *J. Appl. Phys.* **39**, 4662 (1968).

⁹H. Haken, *Phys. Lett. A* **53**, 77 (1975).

¹⁰K. Ikeda, K. Otsuka, and K. Matsumoto, *Progr. Theor. Phys. Suppl.* No. 99, 295 (1989); K. Otsuka, *Phys. Rev. Lett.* **65**, 329 (1990).

¹¹P. C. Hohenberg and B. I. Shraiman, *Physica D* **37**, 109 (1989).

¹²J. V. Moloney, F. A. Hopf, and H. M. Gibbs, *Phys. Rev. A* **25**, 3442 (1982); D. W. Laughlin, J. V. Moloney, and A. C. Newell, *Phys. Rev. Lett.* **51**, 75 (1983); W. J. Firth and E. M. Wright, *Phys. Lett. A* **92**, 211 (1982).

¹³P. Coulet, L. Gil, and F. Lega, *Phys. Rev. Lett.* **62**, 1619 (1989); K. Otsuka and K. Ikeda, "Global chaos in a discrete time-dependent CGL equation," preprint, 1990.

¹⁴For a review of the statistical properties in optical bistability see: L. Lugiato, *Progress in Optics*, edited by E. Wolf (North-Holland, Amsterdam, 1984), Vol. XXI, pp. 69–216.

¹⁵F. T. Arecchi, V. Degiorgio, and B. Querzola, *Phys. Rev. Lett.* **19**, 1168 (1967); F. T. Arecchi and V. Degiorgio, *Phys. Rev. A* **3**, 1108 (1971).

¹⁶R. Kubo, in *Synergetics*, edited by H. Haken (Teubner, Stuttgart, 1973), pp. 28–44.

¹⁷F. Haake, *Phys. Rev. Lett.* **41**, 1685 (1978).

¹⁸(a) F. T. Arecchi and A. Politi, *Phys. Rev. Lett.* **45**, 1219 (1990); (b) F. T. Arecchi, A. Politi, and L. Ulivi, *Nuovo Cimento B* **71**, 119 (1982).

¹⁹R. Roy, A. W. Yu, and S. Zhu, *Phys. Rev. Lett.* **55**, 2794 (1985).

²⁰P. Spano, A. D'Ottavi, A. Mecozzi, and B. Daino, *Appl. Phys. Lett.* **52**, 2203 (1988); A. Mecozzi, S. Piazzolla, A. D'Ottavi, and P. Spano, *Phys. Rev. A* **38**, 3136 (1988).

²¹(a) F. T. Arecchi, R. Meucci, and J. A. Roversi, *Europhys. Lett.* **8**, 225 (1989); (b) F. T. Arecchi, W. Gadoski, R. Meucci, and J. A. Roversi, *Phys. Rev. A* **39**, 4004 (1989).

²²P.-y. Wang, M. Ciofini, R. Meucci, and F. T. Arecchi, "Influence of population inversion noise on the transient statistics of lasers near threshold," submitted to *Phys. Rev. Lett.*

²³F. T. Arecchi, R. Meucci, G. P. Puccioni, and J. R. Tredicce, *Phys. Rev. Lett.* **49**, 1217 (1982).

²⁴F. T. Arecchi and F. Lisi, *Phys. Rev. Lett.* **49**, 94 (1982).

²⁵R. F. Miracky, J. Clarke, and R. H. Koch, *Phys. Rev. Lett.* **50**, 1856 (1983).

²⁶(a) M. R. Beasley, D. D. Humieres, and B. A. Huberman, *Phys. Rev. Lett.* **50**, 1328 (1983); (b) R. Voss, *ibid.* **50**, 1329 (1983); (c) F. T. Arecchi and F. Lisi, *ibid.* **50**, 1330 (1983).

²⁷Ia. G. Sinai, in *Proceedings of the Berlin Conference on Mathematical Problems in Theoretical Physics*, edited by R. S. Schrader, R. Seiler, and D. A. Ohlenbrock (Springer-Verlag, Berlin, 1982), p. 12; E. Marinari, G. Parisi, D. Ruelle, and P. Windey, *Phys. Rev. Lett.* **50**, 1223 (1983).

²⁸C. Grebogi, E. Ott, and J. A. Yorke, *Phys. Rev. Lett.* **49**, 1507 (1982) and *Physica D* **7**, 181 (1983).

²⁹F. T. Arecchi, R. Badii, and A. Politi, *Phys. Rev. A* **29**, 1006 (1984).

³⁰F. T. Arecchi, R. Badii, and A. Politi, *Phys. Lett. A* **103**, 3 (1984).

³¹F. T. Arecchi, R. Badii, and A. Politi, *Phys. Rev. A* **32**, 402 (1985).

³²J. C. Sommerer, E. Ott, and C. Grebogi, *Phys. Rev. A* **43**, 1754 (1991).

³³J. C. Sommerer, C. Grebogi, E. Ott, and M. L. Spano, *Phys. Rev. Lett.* **66**, 1947 (1991).

³⁴A. van der Ziel, *Physica* **16**, 359 (1980).

³⁵E. W. Montroll and M. F. Shlesinger, *Proc. Natl. Acad. Sci. USA* **79**, 3380 (1982).

³⁶G. Grebogi, E. Ott, and J. A. Yorke, *Phys. Rev. Lett.* **50**, 935 (1983); S. M. McDonald, C. Grebogi, E. Ott, and J. A. Yorke, *Physica D* **17**, 125 (1985).

³⁷F. T. Arecchi and S. Califano, *Europhys. Lett.* **3**, 5 (1987).

³⁸P. Bak, C. Tang, and K. Wiesenfeld, *Phys. Rev. Lett.* **59**, 381 (1987); *Phys. Rev. A* **38**, 364 (1988).

³⁹C. Grebogi, E. Ott, and J. A. Yorke, *Phys. Rev. Lett.* **57**, 1284 (1986).

⁴⁰C. Jeffries and J. Perez, *Phys. Rev. A* **27**, 601 (1983); S. K. Brorson, D. Dewey, and P. S. Linsay, *ibid.* **A 28**, 1201 (1983); M. Iansiti, Q. Hu, R. M. Westervelt, and M. Tinkham, *Phys. Rev. Lett.* **55**, 746 (1985).

⁴¹D. Hennequin, P. Glorieux, and D. Dangoisse, *Phys. Rev. Lett.* **57**, 2657 (1986).

⁴²R. Meucci, A. Poggi, F. T. Arecchi, and J. R. Tredicce, *Optics Comm.* **65**, 151 (1988).

⁴³L. P. Shil'nikov, *Dokl. Akad. Nauk SSSR* **160**, 558 (1965); L. P. Shil'nikov, *Mat. Sb.* **77**, 119, 461 (1968); **81**, 92, 123 (1979).

- ⁴⁴A. Arneodo, P. H. Coulet, E. A. Spiegel, and C. Tresser, *Physica D* **14**, 327 (1985).
- ⁴⁵F. T. Arecchi, R. Meucci, and W. Gadomski, *Phys. Rev. Lett.* **58**, 2205 (1987).
- ⁴⁶F. Argoul, A. Arneodo, and P. Richetti, *Phys. Lett. A* **120**, 269 (1987).
- ⁴⁷P. Glendinning and C. Sparrow, *J. Stat. Phys.* **35**, 645 (1984); P. Gaspard, R. Kapral, and G. Nicolis, *ibid.* **35**, 697 (1984).
- ⁴⁸F. T. Arecchi, A. Lapucci, R. Meucci, J. A. Roversi, and P. Coulet, *Europhys. Lett.* **6**, 677 (1988).
- ⁴⁹F. T. Arecchi, W. Gadomski, A. Lapucci, R. Meucci, H. Mancini, and J. A. Roversi, *J. Opt. Soc. Am. B* **5**, 1153 (1988).
- ⁵⁰J. P. Crutchfield, D. Farmer, and B. A. Hubermann, *Phys. Rev.* **92**, 45 (1982).
- ⁵¹F. T. Arecchi, W. Gadomski, and R. Meucci, *Phys. Rev. A* **34**, 1617 (1986).
- ⁵²F. T. Arecchi, G. Giacomelli, P. L. Ramazza, and S. Residori, *Phys. Rev. Lett.* **65**, 2531 (1990).
- ⁵³F. T. Arecchi, G. Giacomelli, P. L. Ramazza, and S. Residori, "Vortices and defect statistics in two-dimensional optical chaos," submitted to *Phys. Rev. Lett.*